CHAPTER IV

RESULTS AND DISCUSSION

The primary goal of this study is to develop a technology with intention of improving the conversion of glycerol and selectivity toward propylene glycol. To achieve this purpose, it is necessary to understand the fundamental chemistry and mechanism behind the dehydroxylation of glycerol to propylene glycol.

There have been two proposed reaction mechanisms for the dehydroxylation of glycerol. First, the glyceraldehydes route (Montassier *et al.*, 1991) involves dehydrogenation of glycerol to glyceric aldehyde in equilibrium with its enolic tautomer, then dehydroxylation reaction, followed by hydrogenation of the intermediate unsaturated aldehyde to propylene glycol. Second, the acetol route (Dasari *et al.*, 2005) involves dehydration of glycerol and further hydrogenate acetol intermediate to propylene glycol.

In the previous study (Swangkotchakorn, 2008), the optimum condition for dehydroxylation reaction was conducted at 250°C, 500 psig, H_2:glycerol of 4:1 over various metal (Cu, Pd, Ni, Co-Mo) on Al_2O_3 support. Among the catalysts tested, the supported copper with 10 wt% loading was found as the most active catalyst for the dehydroxylation of glycerol to propylene glycol. According to the author, the addition of ZnO to Cu/Al_2O_3 could prolong the stability of the catalyst by preventing the formation of aluminum copper and coke deposition.

Primary investigation aims to validate mechanism for the conversion of glycerol to propylene glycol over $CuZnO/Al_2O_3$ catalyst. The dependence of the glycerol conversion upon space velocity as a function of time on stream is given in Figure 4.1. For LHSV of 1.5 h^{-1}, the activity remained unchanged due to the presence of excess catalysts. In case of LHSV beyond 1.5 h^{-1}, the conversion decreases as a function of time on stream. Figure 4.2 shows the plot of selectivity as a function of conversion performed with varied LHSV. It can be indicated that acetol is found only as the reactive intermediate which is then hydrogenated to form propylene glycol. Therefore, the more plausible reaction route is via acetol which proposed by Dasari *et al.*

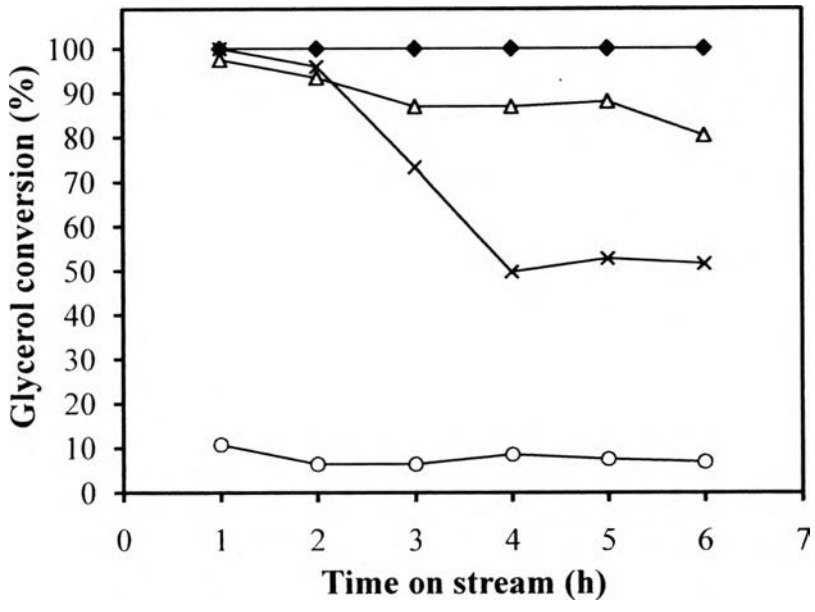

Figure 4.1 Glycerol conversion as a function of time on stream over $CuZnO/Al_2O_3$ catalyst at varied liquid hourly space velocity of (♦) 1.5, (Δ) 3, (×) 6, and (○) 10 h^{-1}.

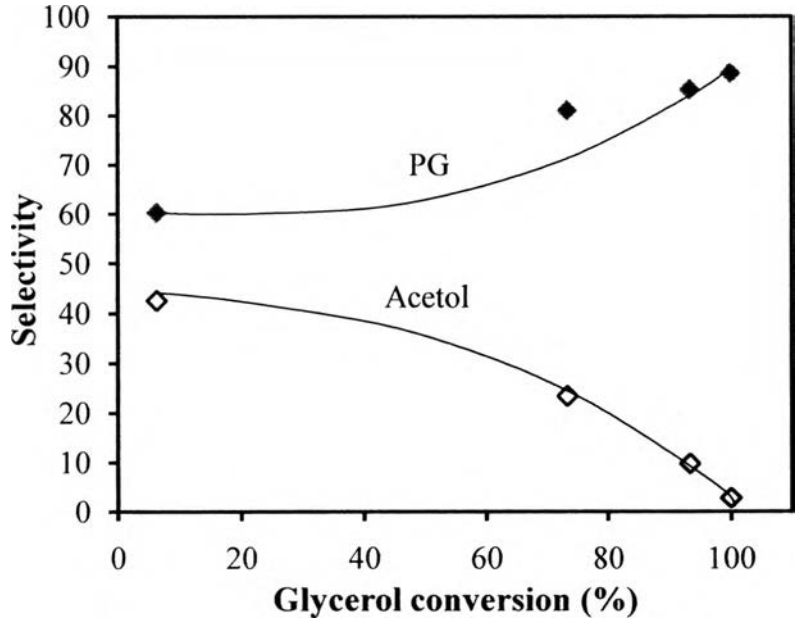

Figure 4.2 Glycerol conversions and selectivities to acetol (○) and propylene glycol (PG) (●) over $CuZnO/Al_2O_3$ catalyst. Reaction condition: 80% glycerol feed, 250°C, 500 psig, H_2: glycerol = 4:1, TOS = 2 h.

According to previous studies, neither Cu/ZnO (without Al_2O_3 support) nor Cu/Al_2O_3 with other promoters has been investigated for this reaction. These considerations led us to compare the catalytic performance between them first. Furthermore, the effects of calcination temperature and catalyst preparation method were then investigated.

4.1 Effect of Promoters

The effect of addition of various promoters (ZnO, Cr_2O_3, CeO_2, Fe_2O_3) to Cu/Al_2O_3 catalyst was investigated. The catalytic activity of Cu/Al_2O_3 and the four different metal oxide-promoted Cu/Al_2O_3 are shown in Figure 4.3. It is clearly seen that the activity were different for the various catalysts, indicating an effect of metal oxides contained in the copper catalysts on the dehydroxylation reaction. The order of metal oxides on the specific activity was ZnO > Cr_2O_3 > CeO_2 > Fe_2O_3. Fierro *et al.* (1996) reported that ZnO is known to improve the dispersion of copper and also its reducibility, which may be important if a redox reaction mechanism occurs. From this result, the $CuZnO/Al_2O_3$ catalyst was chosen for further study.

4.2 Comparison of Catalytic Performance between Cu/Al_2O_3, $CuZnO/Al_2O_3$ and Cu/ZnO

4.2.1 Catalytic Performance on the Dehydroxylation of Glycerol

Table 4.1 shows the conversion of glycerol and selectivities to intermediate acetol and propylene glycol after 6 h of reaction. It is found that neither ZnO nor Al_2O_3 has a promotion effect on conversion of glycerol to propylene glycol. As can be seen in Table 4.1, the glycerol conversion and selectivity to propylene glycol over $CuZnO/Al_2O_3$ catalysts is higher than those obtained from Cu/ZnO and Cu/Al_2O_3 catalysts.

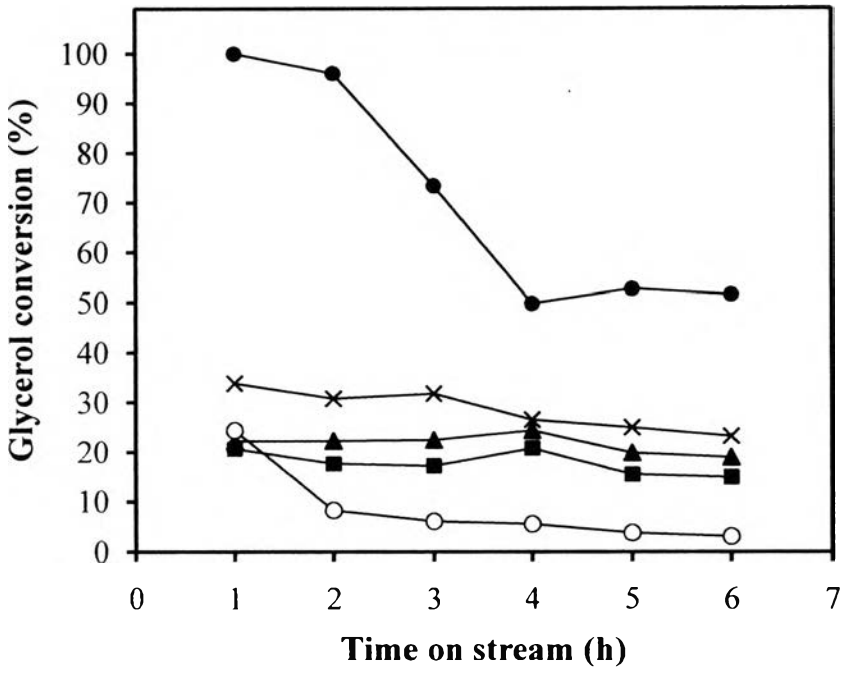

Figure 4.3 Glycerol conversion as a function of time on stream over different kind of promoters on Cu-based catalysts: (○) Cu/Al_2O_3, (●) $CuZnO/Al_2O_3$, (×) $CuCr_2O_3/Al_2O_3$, (▲) $CuCeO_2/Al_2O_3$, and (■) $CuFe_2O_3/Al_2O_3$. Reaction conditions: 80% glycerol feed, 250°C, 500 psig, H_2: glycerol = 4:1, LHSV = 6 h^{-1}.

Table 4.1 Activity and selectivity for dehydroxylation of glycerol over the Cu-based catalysts

Catalyst	Conversion (%)	Selectivity (%)			
		Propylene glycol	Acetol	Ethylene glycol	Isopropanol
Cu/ZnO	6.9	44.4	22.4	3	30.24
Cu/Al_2O_3	3.0	39.3	60.7	0	0
$CuZnO/Al_2O_3$	51.6	48.7	31.29	2.3	0

Reaction conditions: 80% glycerol feed, 250°C, 500 psig, H_2: glycerol = 4:1, LHSV = 6 h^{-1}, TOS = 6 h.

4.2.2 Catalyst Characterization

Table 4.2 provides the BET specific areas of the supports and catalysts. After impregnation of support, it is clearly seen that a decrease in the surface area is observed. Although the surface area of the Cu/Al_2O_3 catalyst is higher than that of the Cu/ZnO and $CuZnO/Al_2O_3$ catalysts, the catalytic activity is quite low. Therefore, the effect of surface area of the catalysts is insignificant for this study.

Table 4.2 BET surface area of the copper-based catalysts

Catalyst	Calcination temperature (°C)	BET surface area (m^2/g)
ZnO	-	9
Al_2O_3	-	262
Cu/ZnO	600	7
Cu/Al_2O_3	600	208
$CuZnO/Al_2O_3$	400	159
	500	180
	600	139
	700	97

In order to examine the reduction behavior of the catalysts, the H_2 TPR studies were carried out in the temperature range from room temperature to 800°C. The TPR profiles of the Cu- and Cu/ZnO-based catalysts are shown in Figure 4.4. In case of the Cu/ZnO catalyst, the low surface area of ZnO support results in large cluster of CuO. It can be suggested that the reduction peak observed at high temperature of 330°C might be associated with the reduction of bulk CuO (Huang *et al.*, 1998). In case of CuO supported on Al_2O_3, TPR results showed two reduction

peaks. The first reduction peak was attributed to the reduction of Cu^{2+} species that are easily reduced. This peak was probably due to the reduction of a well-dispersed CuO phase. The other peak corresponded to less-reducible CuO. This high temperature peak could be related to the reduction of larger CuO particles (Kundakovic and Flytzani-Stephanopoulas, 1998; López-Suárez *et al.*, 2008). The same results were also obtained by Dow *et al.* (1996). They reported that the first peak was ascribed to isolated Cu^{2+} ion, and small two- and three-dimensional clusters. The second peak referred large three-dimensional clusters and bulk CuO phases, which had a character and properties identical to those of pure CuO powder. On the contrary, TPR analysis of the fresh $CuZnO/Al_2O_3$ catalyst showed a sharp reduction peak with additional shoulder, which were attributed to the highly dispersed and small amount of less-reducible CuO species, respectively. When compared the TPR results of the Cu/ZnO (Figure 4.4(d)) and $CuZnO/Al_2O_3$ (Figure 4.4(f)) catalysts, it can be indicated that the aggregation of Cu species was inhibited by the addition of Al species, as reported by Shishido *et al.* (2004). The TPR profiles of Cu/Al_2O_3 catalysts (Figure 4.4(e)) and after ZnO addition (Figure 4.4(f)) were also investigated, it is observed that the second reduction peak of the latter was weaker than that of the former. This result shows that ZnO acts as a stabilizer via dispersing some of CuO crystallites and hindering their grain growth to form bulk CuO, as reported by El-Shobaky *et al.* (1997). Pérez-Hernández *et al.* (2008) reported that the activity of highly dispersed copper is much higher than that of bulk CuO. According to the authors, the higher activity of the $CuZnO/Al_2O_3$ catalyst might be associated with the copper dispersion.

Figure 4.5 (A) and (B) shows XRD pattern of the catalyst before and after reduction with hydrogen, respectively. As can be seen in Figure 4.2(A), both unreduced Cu/ZnO and Cu/Al_2O_3 catalyst show the diffraction lines due to CuO (JCPDS file No. 45-0937). In contrast to bimetallic $CuZnO/Al_2O_3$ catalyst, less intense diffraction lines characteristic of CuO was observed, although the large reduction peak of CuO was observed in TPR results. One explanation is that the crystallite size of CuO is too small to be detected by XRD. It was evidenced for the higher degree dispersion of CuO. After treatment with hydrogen, all catalyst showed the diffraction peaks of metallic copper, which revealed the complete reduction of

CuO to Cu, as shown in Figure 4.5(B). This conclusion is also in agreement with the results reported by El-shobaky and co-workers (El-shobaky *et al.*, 1997). According to the authors, ZnO hinders the solid-solid interaction between CuO and Al_2O_3 and decrease the crystallinity of CuO crystallites which may be taken as evidence for higher degree of dispersion of CuO on Al_2O_3.

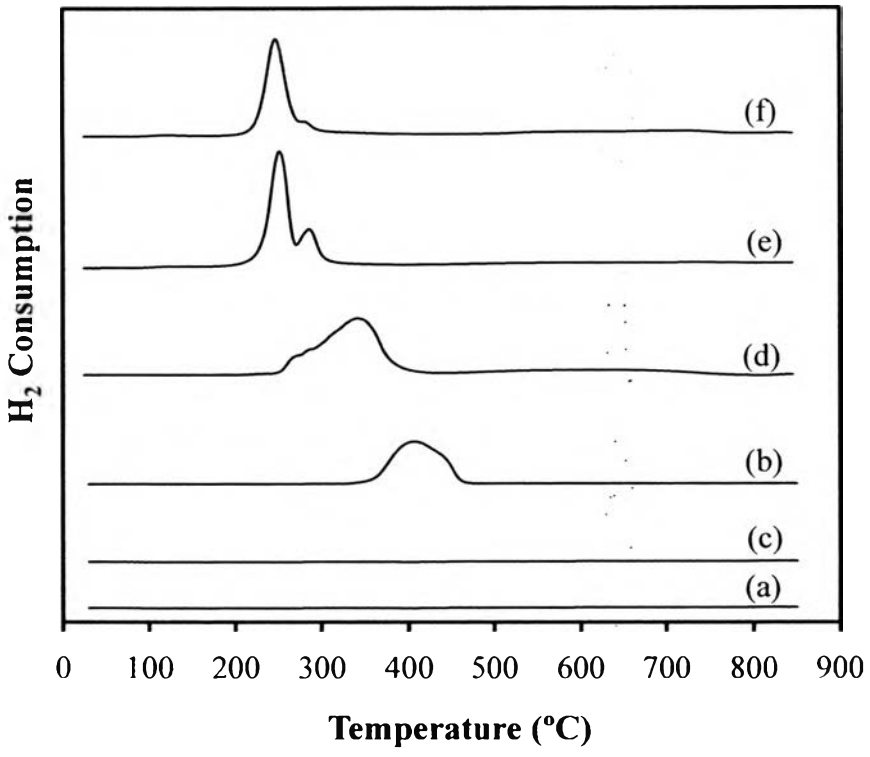

Figure 4.4 TPR profiles of the (a) ZnO, (b) γ-Al_2O_3, (c) CuO, (d) Cu/ZnO, (e) Cu/Al_2O_3, and (f) CuZnO/Al_2O_3 catalysts.

4.3 Effect of Calcination Temperature of the CuZnO/Al_2O_3 Catalysts

4.3.1 Catalytic Activity Measurement

The activities of the impregnated CuZnO/Al_2O_3 catalysts prepared at different calcination temperatures (400–700°C) are shown in Figure 4.6. Among the catalyst tested, it is found that the catalyst calcined at 500°C shows the best activity and stability, while the other catalysts show an abrupt degradation in activity.

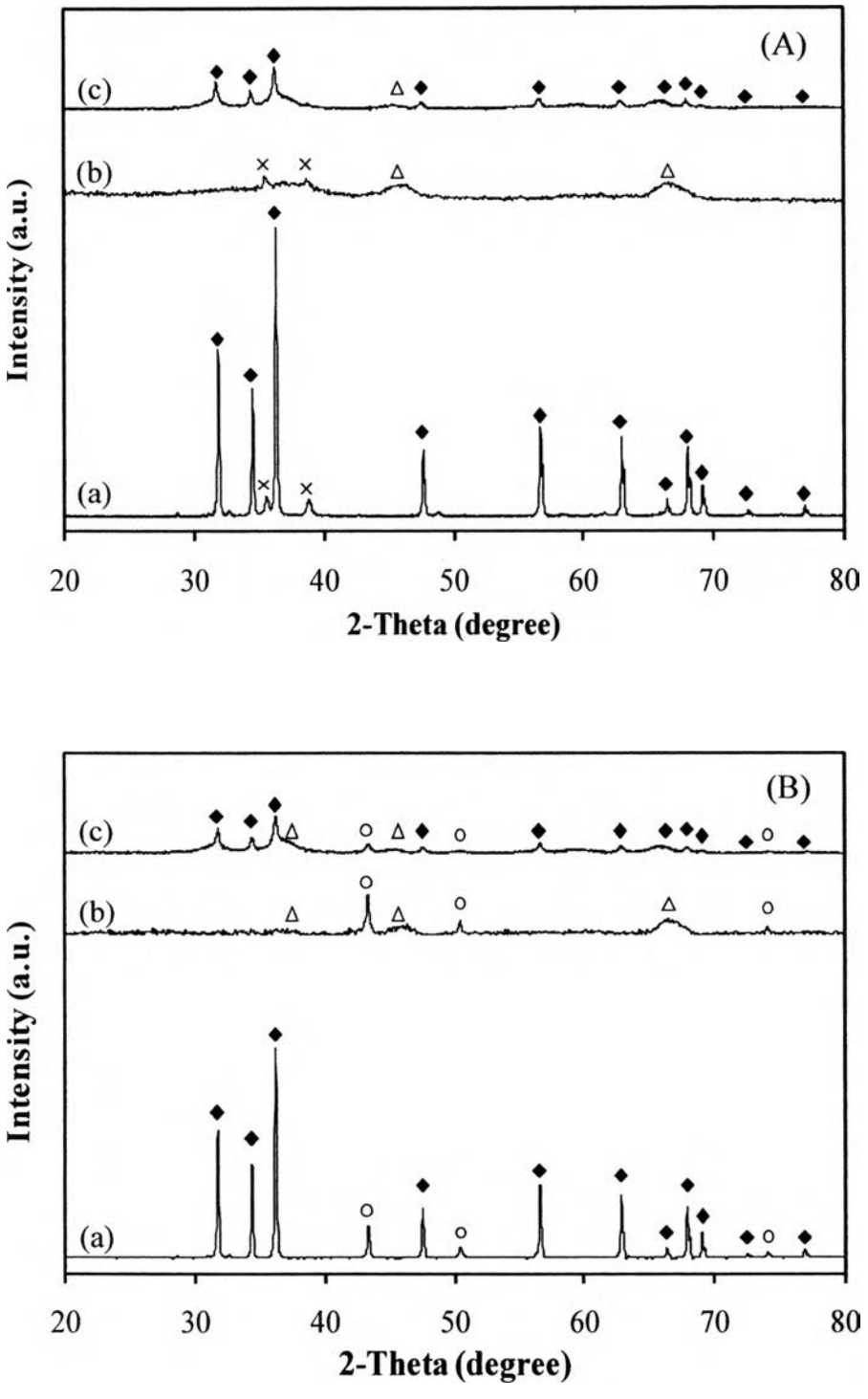

Figure 4.5 XRD patterns of the (a) Cu/ZnO, (b) Cu/Al_2O_3, and (c) $Cu/ZnO/Al_2O_3$, (A) before and (B) after reduction with H_2. (×) CuO; (○) Cu; (♦) ZnO; and (Δ) Al_2O_3.

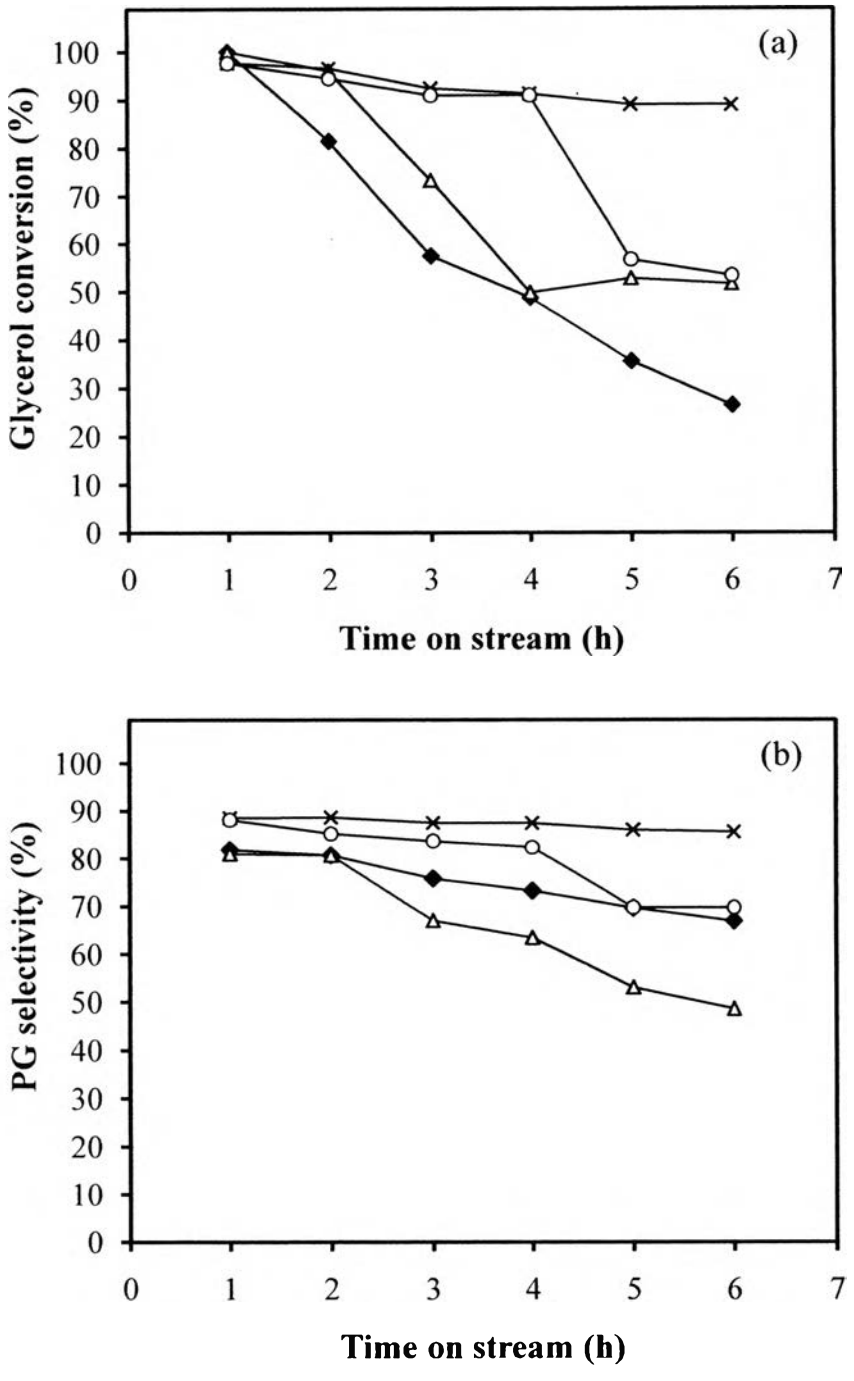

Figure 4.6 (a) Glycerol conversion and (b) selectivity to propylene glycol as a function of time on stream for the $Cu/ZnO/Al_2O_3$ catalysts calcined at different temperatures: (○) 400°C, (×) 500°C, (Δ) 600°C, and (♦) 700°C.

4.3.2 Catalyst Characterization

The BET specific surface areas of the catalysts calcined at 400–700°C are summarized in Table 4.1. It can be observed that, except for catalyst calcined at 400°C, the BET surface area of the $CuZnO/Al_2O_3$ catalysts gradually decreased with an increase in calcination temperature. The low BET surface area of the catalyst calcined at 400°C might be attributed to the presences of uncalcined copper precursor as shown in TGA and TPR profiles later.

The TG-DTA of uncalcined $CuZnO/Al_2O_3$ catalyst is shown in Figure 4.7. It is evident that all adsorbed and bound water and precursor are completely decomposed around 450°C. Therefore, some precursors still remain for the catalyst calcined at 400°C. This is a reason why the catalyst has a low BET surface area as shown in Table 4.2.

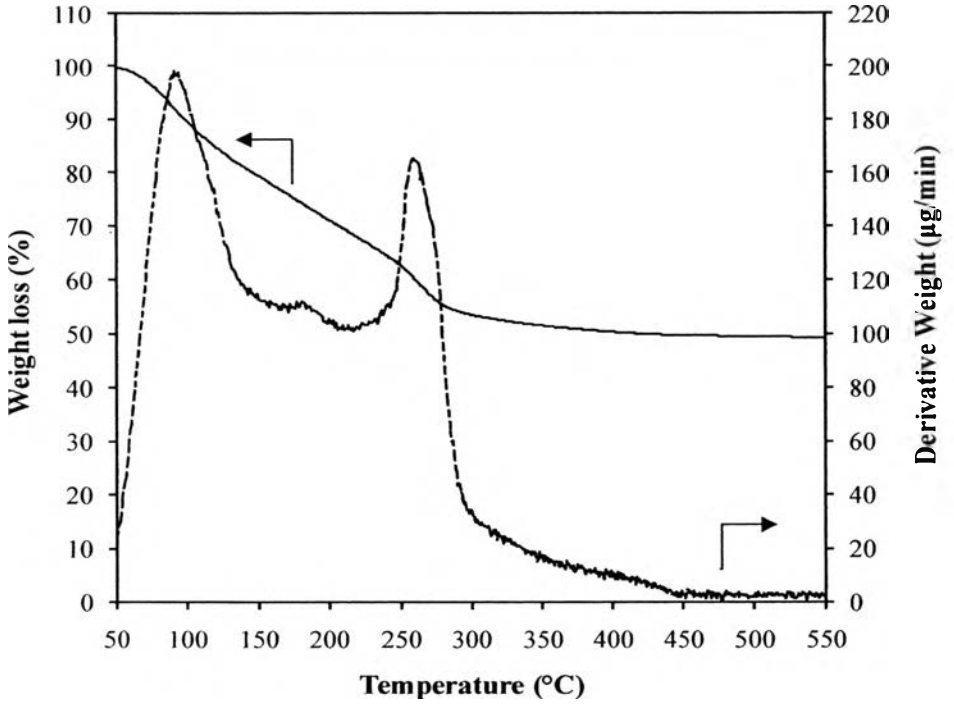

Figure 4.7 TG-DTA of uncalcined $CuZnO/Al_2O_3$ catalyst. (–) weight loss, (--) derivative weight.

The H_2-TPR profiles of the catalysts are shown in Figure 4.8. All catalysts showed two reduction peaks. The first peak is attributed to the reduction of highly dispersed CuO species, and the second at higher temperature is assigned to the reduction of CuO which was the stronger interaction with ZnO and/or Al_2O_3 support. In addition, for the catalysts calcined at 400°C, a large broad peak in the range of 300–500°C is observed indicating the reduction peak of uncalcined Cu precursor. With increasing calcinations temperature, the position of that peaks shifts to lower temperature which might be attributed to the formation of the Cu^{2+} ion in a distorted octahedral geometry of $CuAl_2O_4$ surface spinels which has been observed at much lower temperatures (Marchi *et al.*, 2003).

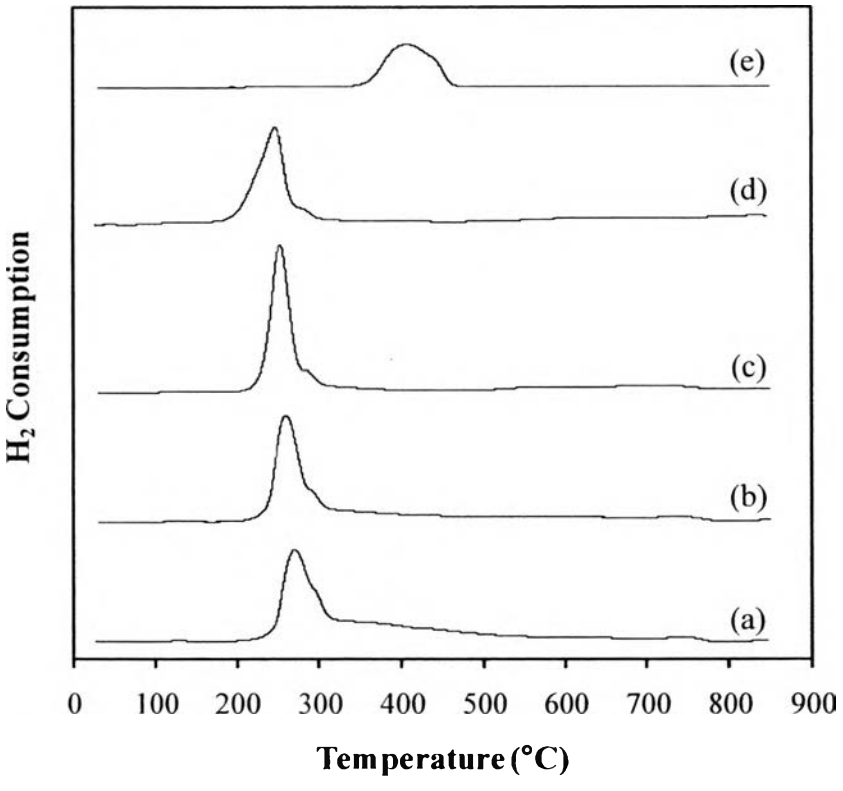

Figure 4.8 TPR profiles of the impregnated $CuZnO/Al_2O_3$ catalysts calcined at different temperatures: (a) 400°C, (b) 500°C, (c) 600°C, (d) 700°C and (e) reference standard CuO.

XRD patterns of the fresh $CuZnO/Al_2O_3$ catalysts calcined at 400–700°C are illustrated in Figure 4.9. It can be observed that no or less intense XRD diffraction lines characteristic of CuO is observed for all catalysts, although the reduction peak of CuO with a significantly large intensity is detected in TPR measurement. For the catalyst calcined 700°C, the experimental results showed the new board lines that can be assigned to the aluminate-like spinel species.

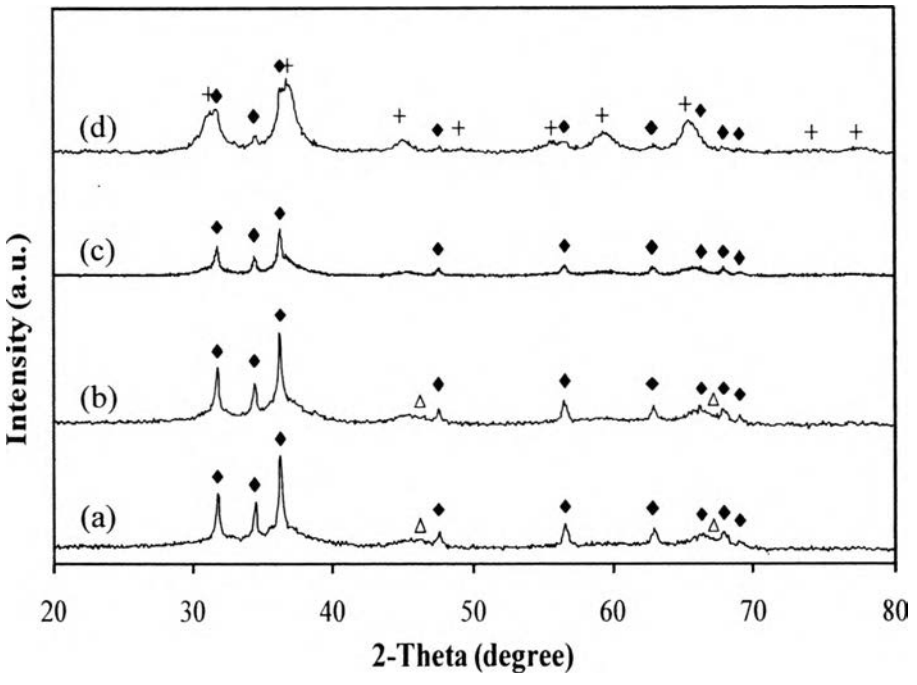

Figure 4.9 XRD patterns of the unreduced $CuZnO/Al_2O_3$ catalysts prepared at different calcinations temperature: (a) 400°C, (b) 500°C, (c) 600°C, and (d) 700°C. (○) Cu; (♦) ZnO; (■) Al_2O_3; and (+) $ZnAl_2O_4$.

Figure 4.10 shows the XRD pattern of the catalysts reduced by H_2 at 300°C for 1 h. All catalysts demonstrate that the complete reduction of CuO by H_2 takes place to yield metallic copper. On the other hand, no change in the diffraction lines due to spinel-like phase is observed before and after treatment with H_2. This result reveals that this species is hardly reduced by H_2 below 300°C, as pointed out by Fuangnawakij *et al.* (2008).

By combining the result from BET, XRD, and TPR measurements, it can be suggested that a better performance of the catalyst calcined at 500°C might be attributed to the high BET surface area and ascribed to the dispersion of CuO species. It also appears that with increasing the calcination temperatures above 400°C, the decrease in the conversion is associated with decreasing the specific surface area, which can result in losing the active sites.

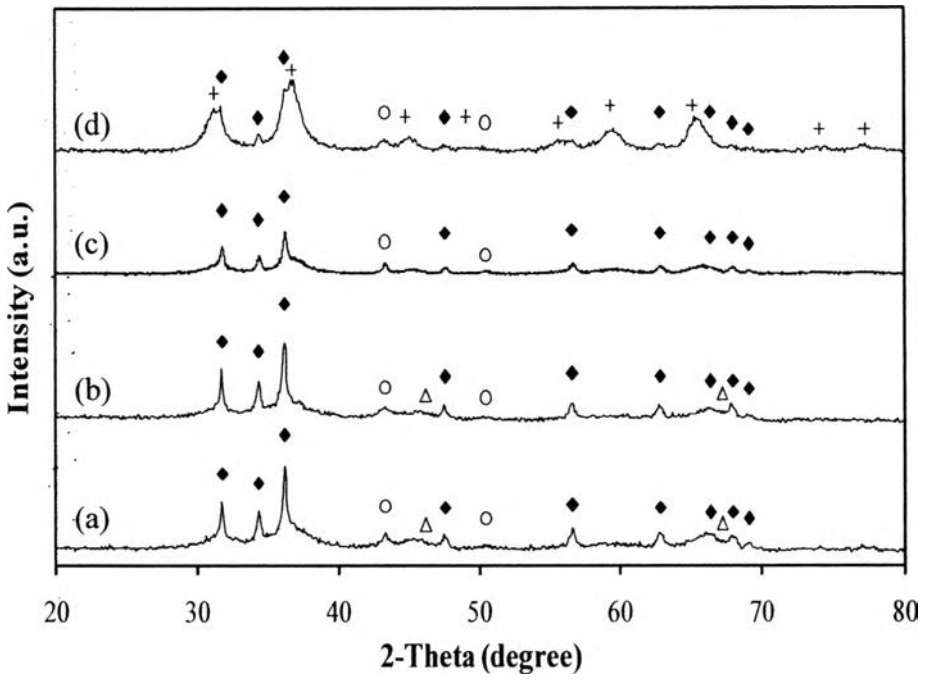

Figure 4.10 XRD patterns of the reduced $CuZnO/Al_2O_3$ catalysts prepared at different calcinations temperature: (a) 400°C, (b) 500°C, (c) 600°C, and (d) 700°C. (○) Cu; (♦) ZnO; (Δ) Al_2O_3; and (+) $ZnAl_2O_4$.

4.4 Effect of Catalyst Preparation Method

4.4.1 Catalytic Activity of the Impregnated and Co-precipitated Catalysts

In this study, the activities of catalysts prepared by different procedures are compared for incipient wetness impregnation and co-precipitation as shown in Figure 4.11. Both catalysts were calcined at the same temperature of 500°C. The experimental results demonstrate that the activity of the impregnated catalyst is

similar to that of the co-precipitated catalyst at the initial stage of the reaction, but subsequently a gradual degradation is observed.

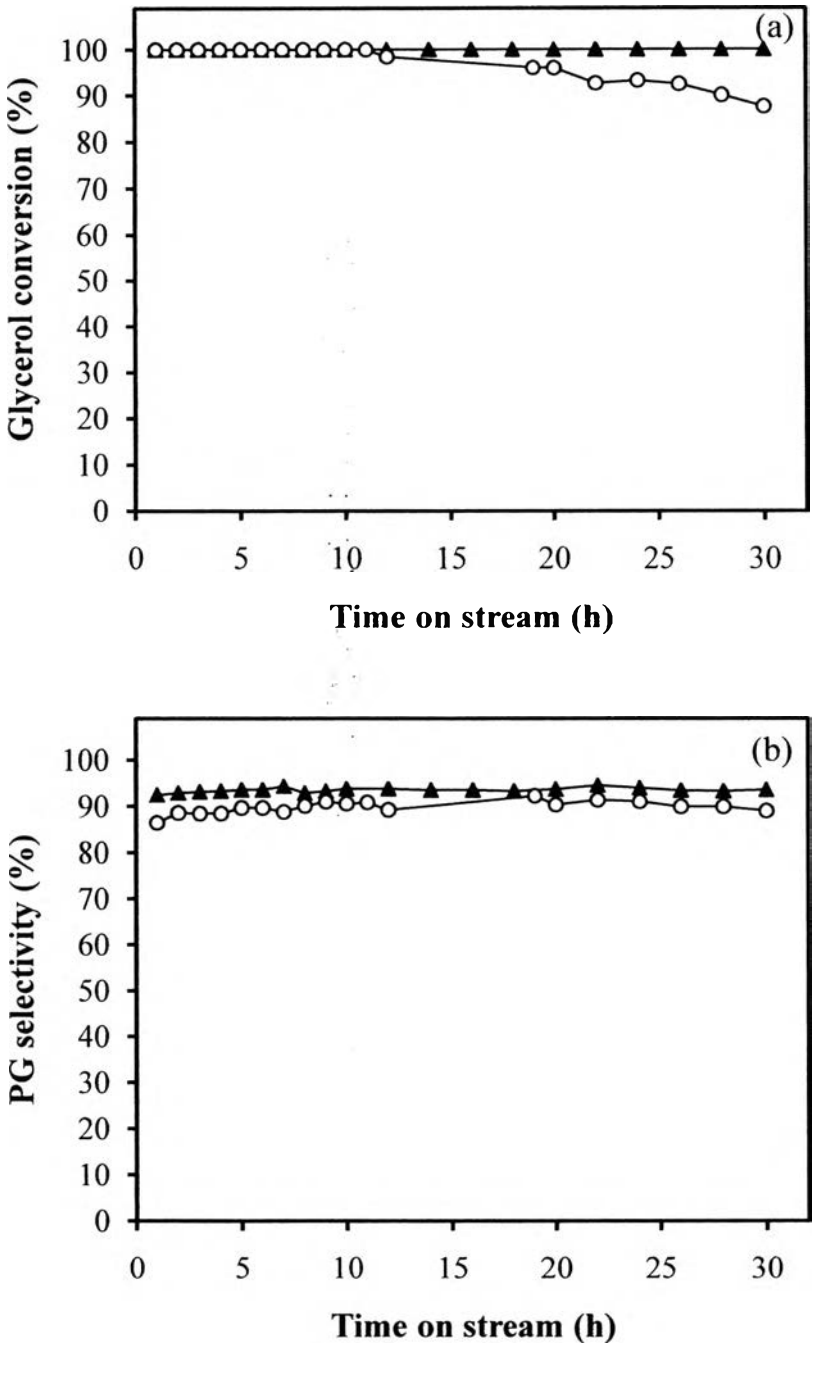

Figure 4.11 Time course of (a) conversion of glycerol and (b) selectivities to propylene glycol over $CuZnO/Al_2O_3$ catalysts prepared by different preparation

methods: (○) incipient wetness impregnation, and (▲) co-precipitation. Reaction conditions: 250°C, 500 psig, H_2:glycerol = 4:1, and LHSV = 1.5 h^{-1}.

4.4.2 Catalyst Characterization

The compositions and surface area of the catalysts investigated in the present study are summarized in Table 4.3. The catalysts prepared by the impregnation and co-precipitation are hereafter denoted as IMP and COP, respectively

Table 4.3 Compositions and BET surface areas of the catalyst tested

Catalyst	Composition (wt%)*			BET surface area (m^2/g)
	Cu	Zn	Al	
IMP	9.7	30.1	13.1	180
COP	11.6	43.5	8.0	118

*Determined by XRF.

As can be seen in Table 4.3, the BET surface area of the co-precipitated catalyst was lower than that of impregnated catalyst. This is likely due to the differences in the morphologies of the catalysts as a result of their synthesis methods. This reason is supported by SEM micrographs as discussed later. In spite of the lower BET surface area than those prepared by incipient wetness impregnation, the catalyst prepared by co-precipitation showed a higher stability. Therefore, the surface area is not significant parameter for this study.

The H_2-TPR profiles of the catalysts are shown in Figure 4.12. For the co-precipitated catalyst, a sharp single peak is observed indicating the reduction peak of homogeneous dispersed CuO species. However, the reduction peak appears at higher temperature than those of the impregnated catalyst which can be attributed to more interaction between CuO and ZnO and/or Al_2O_3 support.

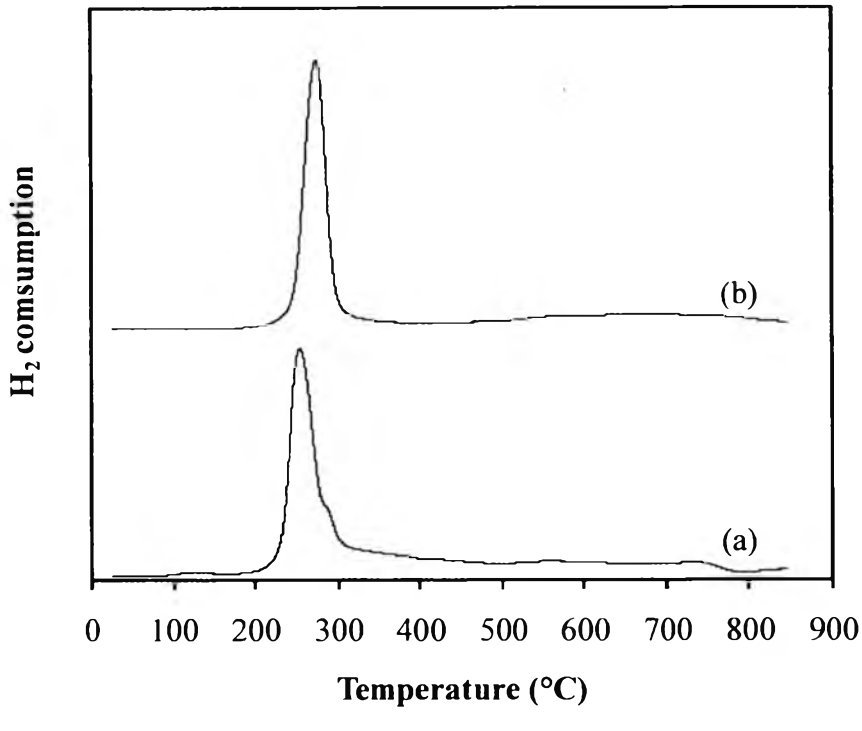

Figure 4.12 TPR profiles of the (a) impregnated, and (b) co-precipitated $CuZnO/Al_2O_3$ catalysts.

The SEM micrographs of the impregnated and co-precipitated catalysts are illustrated in Figure 4.13(a) and (b), respectively. The morphology of the impregnated catalyst is found as large and small spongy clusters. In contrast, the catalyst prepared by co-precipitation method shows the flake-like structure. This image is in agreement with the BET result in the co-precipitated catalyst had a lower surface area than the impregnated.

Figure 4.14(a) and (b) shows TEM images of the impregnated and co-precipitated catalysts, respectively. The rod-like structure found in impregnated catalyst was attributed to the characteristics of alumina support. Figure 4.12(b) shows the co-precipitated catalyst have a relatively uniform particle size distribution, which are too small to be clearly observed with the TEM used in this study. These particles thus were allowing the accessibility of the reactant to precede the reaction at its surface of the catalyst.

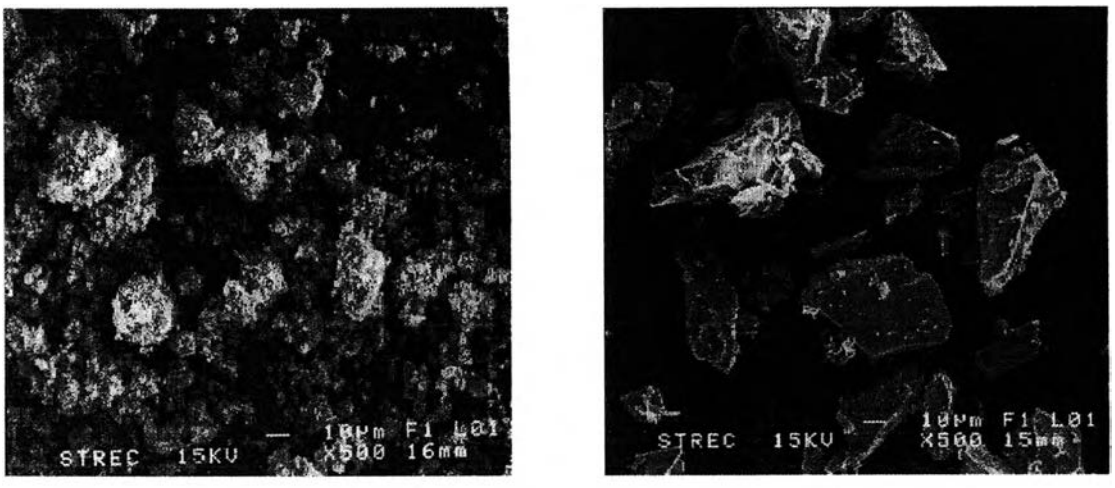

(a) (b)

Figure 4.13 SEM micrographs of the fresh $CuZnO/Al_2O_3$ catalysts prepared by different method; (a) incipient wetness impregnation, and (b) co-precipitation.

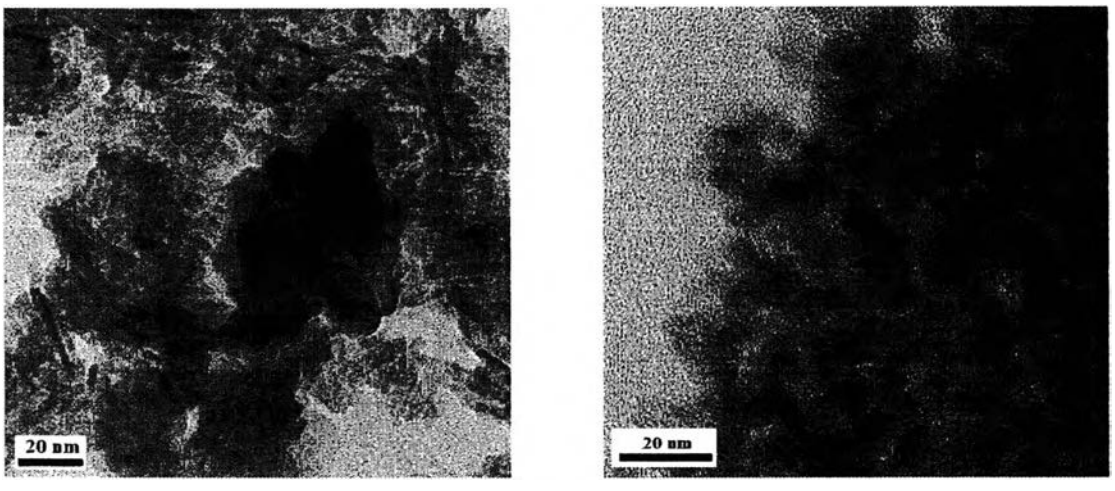

(a) (b)

Figure 4.14 TEM images of the fresh $CuZnO/Al_2O_3$ catalysts prepared by different method; (a) incipient wetness impregnation, and (b) co-precipitation.

The XRD patterns of unreduced, reduced, and spent co-precipitated catalysts are shown in Figure 4.15. All samples exhibited diffraction patterns consistent with the presence of spinel-like phases. Although the large amount of CuO and ZnO are detected in the TPR result, no segregation of both crystalline phases are

detected in Cu–Zn–Al mixed oxide, thereby indicating that both species are highly dispersed in the spinel-like matrix. This result is in agreement with the TEM image, which shows the uniform distribution of the particle. It can be observed that there is no change in diffraction patterns even after the reaction for 30 h, indicating that the crystalline phases of co-precipitated catalyst are more stable when compared with those of impregnated catalyst. By combining the XRD and TEM results, the crystalline phases and morphology of the highly dispersed co-precipitated catalysts is likely reasons for their apparent greater stability over the impregnated catalysts.

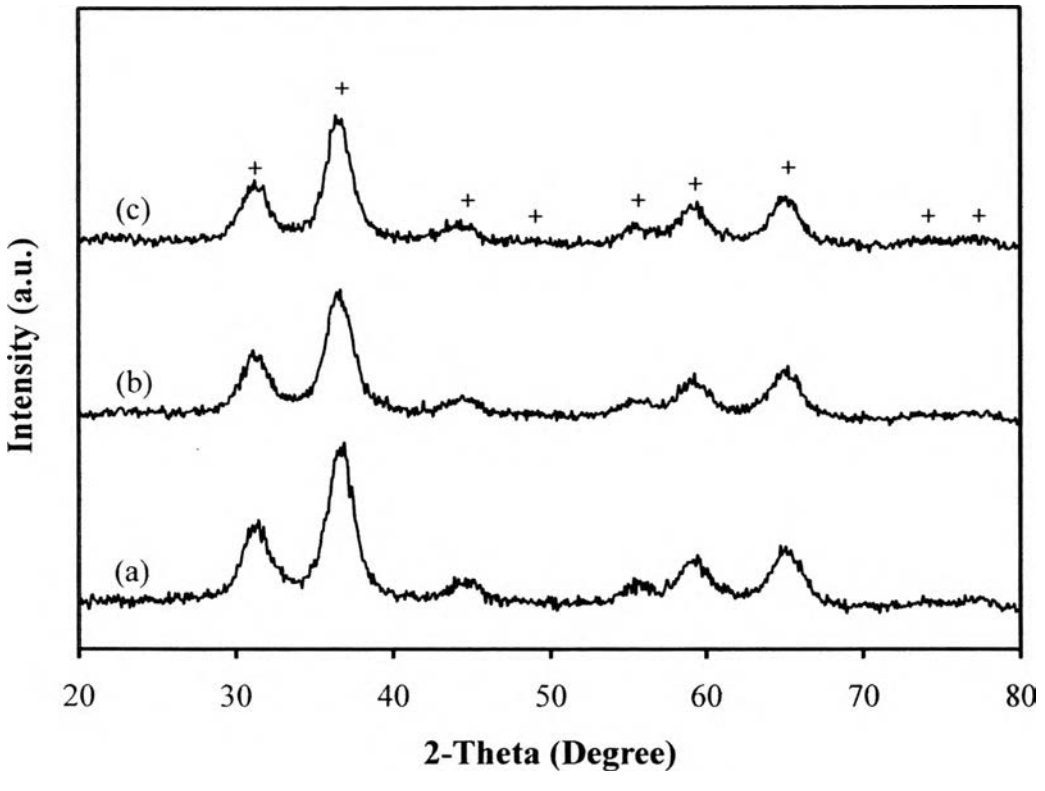

Figure 4.15 XRD patterns of the (a) fresh, (b) reduced, and (c) spent $CuZnO/Al_2O_3$ catalyst prepared by co-precipitation method. (+) $ZnAl_2O_4$.

Figure 4.16 shows the Cu K-edge XANES spectra of the Cu-based catalysts before reduction and the reference CuO compound. A weak pre-edge ascribed to a dipole-forbidden transition of 1s → 3d orbital (Shisido *et al.*, 2006) appears around 8984 eV for the Cu^{2+} species in CuO (Cu^{2+} in a square planar

symmetry). All catalysts showed the weaker peak intensity at 8984 eV than those of CuO, suggesting that the Cu^{2+} in the catalysts possesses the octahedral coordination less distorted than those in CuO.

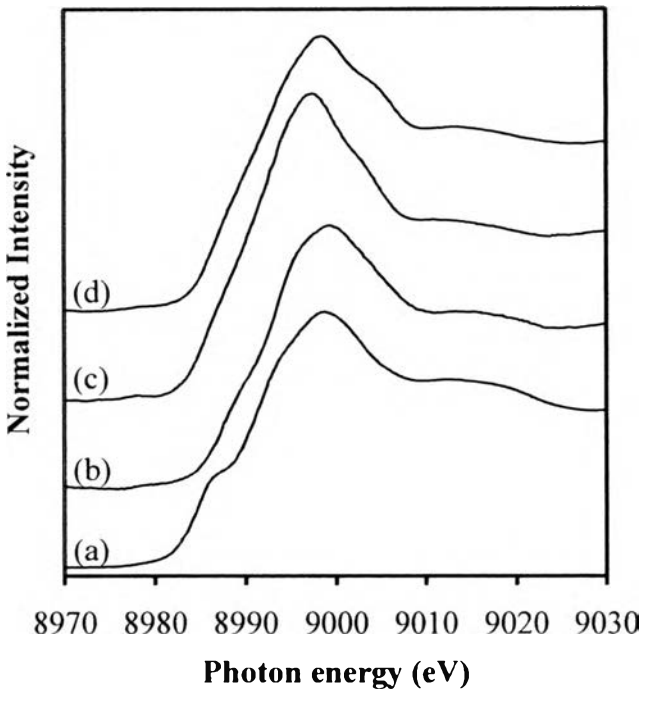

Figure 4.16 Cu K-edge XANES spectra of the fresh copper-based catalysts; (a) CuO, (b) Cu/Al_2O_3, and $CuZnO/Al_2O_3$ catalysts prepared by (c) incipient wetness impregnation, and (d) co-precipitation.

Figure 4.17 shows the Cu K-edge XANES spectra of the reduced Cu-based catalysts and the reference Cu foil compound. Cu foil showed the edge at 8979 eV and two characteristics peaks at higher energy (Velu *et al.*, 1990). All catalysts showed the pre-edge peak, indicating the reduction of CuO to metallic Cu.

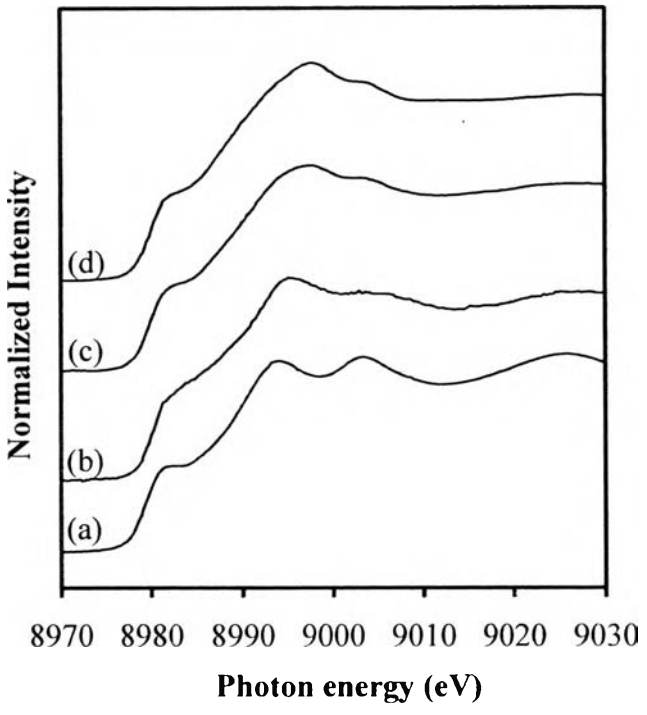

Figure 4.17 Cu K-edge XANES spectra of the reduced copper-based catalysts; (a) Cu foil, (b) Cu/Al_2O_3, and $CuZnO/Al_2O_3$ catalysts prepared by (c) incipient wetness impregnation, and (d) co-precipitation.

Zn K-edge XANES spectra of the impregnated and co-precipitated $CuZnO/Al_2O_3$ catalysts after calcination and reference compounds are shown in Figure 4.18 (A). ZnO shows an edge at 9661 eV and two peaks at 9669 and 9680 eV (Shisido *et al.*, 2006). The impregnated catalyst shows a ZnO-like structure, whereas a $ZnAl_2O_4$-like structure is found for the co-precipitated catalyst. After reaction of 30 h (Figure 4.18 (B)), the impregnated catalyst shows the change from ZnO-like structure to $ZnAl_2O_4$-like structure, while the structure of the co-precipitated catalyst remains the same as previous. All results are in agreement with the XRD patterns as mention above.

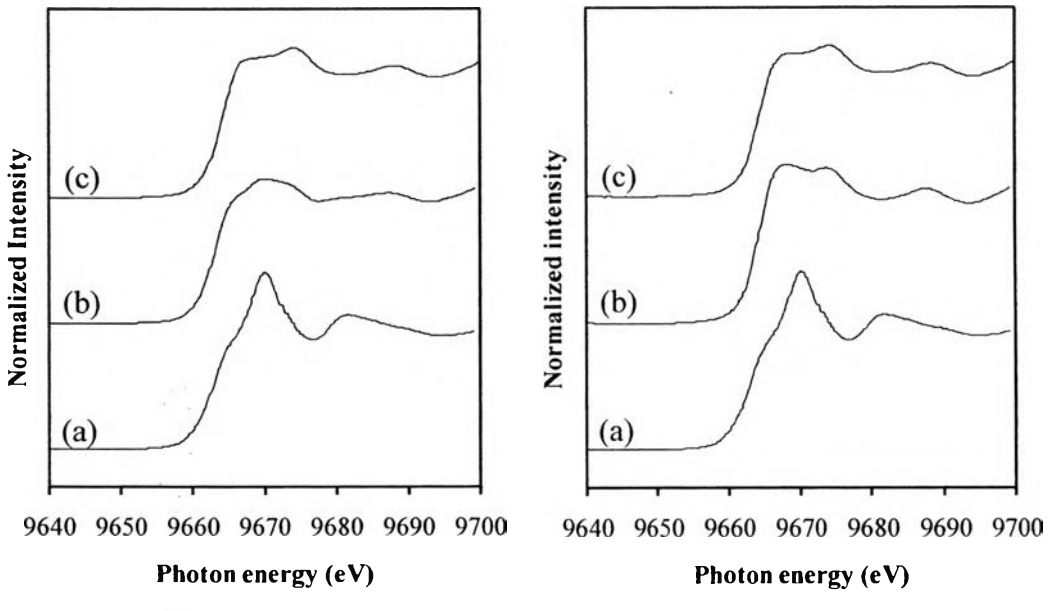

(A) (B)

Figure 4.18 Zn K-edge XANES spectra of the (A) fresh and (B) spent $CuZnO/Al_2O_3$catalysts prepared by different methods; (a) standard ZnO, (b) impregnated, and (c) co-precipitated $CuZnO/Al_2O_3$ catalyst.